

REPORT

Checkpoint signaling and error correction require regulation of the MPS1 T-loop by PP2A-B56

Daniel Hayward¹ , James Bancroft¹, Davinderpreet Mangat^{1*}, Tatiana Alfonso-Pérez^{2*} , Sholto Dugdale¹, Julia McCarthy¹, Francis A. Barr² , and Ulrike Gruneberg¹ 

During mitosis, the formation of microtubule–kinetochore attachments is monitored by the serine/threonine kinase monopolar spindle 1 (MPS1). MPS1 is recruited to unattached kinetochores where it phosphorylates KNL1, BUB1, and MAD1 to initiate the spindle assembly checkpoint. This arrests the cell cycle until all kinetochores have been stably captured by microtubules. MPS1 also contributes to the error correction process rectifying incorrect kinetochore attachments. MPS1 activity at kinetochores requires autophosphorylation at multiple sites including threonine 676 in the activation segment or “T-loop.” We now demonstrate that the BUBR1-bound pool of PP2A-B56 regulates MPS1 T-loop autophosphorylation and hence activation status in mammalian cells. Overriding this regulation using phosphomimetic mutations in the MPS1 T-loop to generate a constitutively active kinase results in a prolonged mitotic arrest with continuous turnover of microtubule–kinetochore attachments. Dynamic regulation of MPS1 catalytic activity by kinetochore-localized PP2A-B56 is thus critical for controlled MPS1 activity and timely cell cycle progression.

Introduction

Generation of the spindle assembly checkpoint (SAC) response depends on the activity of a conserved protein kinase, monopolar spindle 1 (MPS1; [Stucke et al., 2002](#); [Liu and Winey, 2012](#); [Pachis and Kops, 2018](#)). MPS1 localizes to unattached kinetochores and initiates the multisite phosphorylation of the kinetochore protein KNL1 and the SAC proteins BUB1 and MAD1 ([Ciliberto and Hauf, 2017](#); [Faesen et al., 2017](#); [Ji et al., 2017](#)). This promotes the recruitment of SAC proteins to unattached kinetochores and thus the generation of a checkpoint response ([Musacchio, 2015](#)). Clustering of several MPS1 molecules at unattached kinetochores is thought to promote trans autophosphorylation and hence kinase activity ([Kang et al., 2007](#); [Dodson et al., 2013](#); [Combes et al., 2018](#)). This activation step involves autophosphorylation of its T-loop on threonine 676 (T676; [Kang et al., 2007](#); [Mattison et al., 2007](#); [Jelluma et al., 2008a](#)). MPS1 is released upon microtubule binding to kinetochores ([Jelluma et al., 2010](#)), leading to the termination of the checkpoint response and presumably removal of these activating phosphorylations.

Despite this understanding, the phosphatases acting on MPS1 and other checkpoint proteins still need to be clarified. Both PP2A-B56 and PP1 have been implicated in KNL1 dephosphorylation and SAC silencing ([Espert et al., 2014](#); [Nijenhuis et al., 2014](#)). PP1 has been shown to dephosphorylate the MPS1 T-loop in flies ([Moura et al., 2017](#)), but it is not clear whether this

mechanism is conserved in mammals. PP2A-B56 exists in several spatially distinct populations in mammalian mitotic cells ([Qian et al., 2013](#); [Vallardi et al., 2019](#)). One pool is bound to the C-terminal domain of BUBR1 via a conserved LxxIxE motif ([Hertz et al., 2016](#)). This pool of PP2A-B56 has been shown to oppose both Aurora B and MPS1 in chromosome alignment and SAC signaling, respectively ([Suijkerbuijk et al., 2012](#); [Kruse et al., 2013](#); [Xu et al., 2013](#); [Espert et al., 2014](#)). In addition to orchestrating SAC signaling, MPS1 also contributes directly to the turnover of erroneous microtubule–kinetochore attachments by phosphorylating the Ska complex at microtubule–kinetochore junctions. This activity of MPS1 is also opposed by PP2A-B56 ([Maciejowski et al., 2017](#)).

Here we investigate this complex network of phosphatases and find that the BUBR1-dependent pool of PP2A-B56 is the key MPS1 T-loop phosphatase. Furthermore, we demonstrate that dynamic turnover of MPS1 T-loop phosphorylation by PP2A-B56 is crucial for both the SAC and error correction pathways.

Results and discussion

MPS1 T-loop phosphorylation is controlled by PP2A

MPS1 activity is dynamically regulated by autophosphorylation at T676 in the T-loop of the kinase domain ([Kang et al., 2007](#);

¹Sir William Dunn School of Pathology, University of Oxford, Oxford, UK; ²Department of Biochemistry, University of Oxford, Oxford, UK.

*D. Mangat and T. Alfonso-Pérez contributed equally to this paper; Correspondence to Ulrike Gruneberg: ulrike.gruneberg@path.ox.ac.uk.

© 2019 Hayward et al. This article is distributed under the terms of an Attribution–Noncommercial–Share Alike–No Mirror Sites license for the first six months after the publication date (see <http://www.rupress.org/terms/>). After six months it is available under a Creative Commons License (Attribution–Noncommercial–Share Alike 4.0 International license, as described at <https://creativecommons.org/licenses/by-nc-sa/4.0/>).

(Mattison et al., 2007; Jelluma et al., 2008a). To identify the class of phosphatase acting at this site, mitotic HeLa cells expressing endogenously tagged MPS1-GFP were pretreated with PPP family phosphatase inhibitors, and then briefly incubated with MPS1 inhibitor (MPS1i) to stop T-loop autophosphorylation (Ishihara et al., 1989; Mitsuhashi et al., 2001; Hewitt et al., 2010; Choy et al., 2017; Alfonso-Pérez et al., 2019). In control cells, MPS1i resulted in loss of the MPS1 pT676 signal (Fig. 1, A and B; and Fig. S1, A and B). The level of total MPS1-GFP increased, as reported before (Hewitt et al., 2010; Jelluma et al., 2010; Santaguida et al., 2010; Fig. 1, A and C). Addition of a dual PP1/2A inhibitor (PP1/2Ai; calyculin A) but not PP1 inhibitor (PP1i; tautomycin) prevented the loss of the pT676 signal (Fig. 1, A and B). Neither treatment affected the increase of MPS1-GFP levels at kinetochores upon MPS1 inhibition (Fig. 1, A and C). Similar results were obtained in untransformed human telomerase reverse transcriptase-immortalized retinal pigment epithelial cells (RPE-1; Fig. S1, C–E), indicating that these findings were independent of the transformation status of the cells. Taken together, these data suggest that in mammalian cells, in contrast to *Drosophila melanogaster*, a PPP family phosphatase other than PP1 was involved in the turnover of the MPS1 T-loop phosphorylation.

BUBR1-bound PP2A-B56 regulates MPS1 T676 phosphorylation

Since the BUBR1-associated pool of the PP2A-B56 phosphatase had already been identified as the phosphatase acting on several MPS1 autophosphorylations and on MPS1 kinetochore substrates (Espert et al., 2014; Maciejowski et al., 2017; Qian et al., 2017), this form of PP2A was the most likely candidate for the MPS1 T676 PP2A phosphatase complex. Confirming this, depletion of the PP2A catalytic subunit or all B56 subunits resulted in retention of pT676 staining upon MPS1 inhibition (Fig. 1, D–F; Fig. S1, F–H; and Fig. S2, A and B). By contrast, depletion of PP1 catalytic subunits or B55 regulatory subunits had no effect (Fig. 1, D and E; and Fig. S1, F and G). This outcome was seen in both cells arrested in mitosis by addition of nocodazole and mitotic cells during an unperturbed cell cycle (Fig. S2, D and E). Furthermore, in cells expressing the PP2A-B56 binding-defective GFP-BUBR1^{L669A/I672A}, but not WT BUBR1, MPS1 T-loop phosphorylation was retained upon MPS1 inhibition (Kruse et al., 2013; Espert et al., 2014; Fig. 1, G–I; and Fig. S2 C). Since PP2A-B56 also opposes the MPS1-mediated MELT phosphorylations of KNL1 required for BUBR1 kinetochore localization, the PP2A-B56 binding-deficient BUBR1 was retained at the kinetochore as well when MPS1 was inhibited (Espert et al., 2014). Together, these data demonstrate that during mitosis, MPS1 T-loop phosphorylation is dynamically controlled by BUBR1-bound PP2A-B56 (Fig. 1 J).

PP2A-B56 modulates MPS1 kinetochore localization by counteracting both MPS1 and Aurora B

MPS1 localization to unattached kinetochores is promoted by CDK1-CCNB1 and Aurora B and is opposed by its own activity (Hewitt et al., 2010; Jelluma et al., 2010; Santaguida et al., 2010; Saurin et al., 2011; Nijenhuis et al., 2013; Zhu et al., 2013; Hayward et al., 2019). Release of active MPS1 from kinetochores

has been suggested to be triggered by autophosphorylation of the MPS1 N-terminus (Wang et al., 2014). We tested whether the phosphorylation status of T33 and S37 in the N-terminus of MPS1 was also regulated by PP2A-B56. In agreement with a published report, depletion of PP2A-B56 stabilized pT33/pS37 in the absence of MPS1 activity (Fig. 2, A–F; Maciejowski et al., 2017). Surprisingly, this did not result in decreased total MPS1-GFP at kinetochores (Fig. 2, A–F), suggesting that MPS1 self-ejection via autophosphorylation of its N-terminus cannot be the only mechanism determining MPS1 kinetochore levels.

Aurora B is a major positive regulator of MPS1 localization to kinetochores (Santaguida et al., 2010; Saurin et al., 2011; Nijenhuis et al., 2013; Zhu et al., 2013), and it is thus possible that PP2A-B56 simultaneously counteracts the MPS1 N-terminal autophosphorylations promoting MPS1 kinetochore release and the Aurora B-dependent kinetochore phosphorylations promoting MPS1 kinetochore accumulation. Analysis of MPS1-GFP localization in cells treated with Aurora B inhibitor confirmed that MPS1-GFP was lost from kinetochores upon Aurora B inhibition, and that this was prevented by depletion of the PP2A catalytic subunit or all PP2A-B56 regulatory subunits (Fig. 2, G and H). PP2A-B56 therefore opposes Aurora B-mediated MPS1 kinetochore recruitment and hence counters MPS1 self-ejection triggered by the N-terminal autophosphorylation. Consequently, simultaneous inhibition of AURKB and MPS1 in PP2A-B56-depleted cells resulted in MPS1 levels similar to control cells (Fig. 2, I–K).

MPS1-T675D/T676D is an active MPS1 kinase

To study the relevance of MPS1 T-loop regulation by PP2A-B56 in isolation from other substrates, we generated MPS1 mutants in which both the canonical T-loop residue T676 as well as the adjacent threonine T675 were replaced by phosphomimetic aspartate (MPS1^{DD}) or nonphosphorylatable alanine (MPS1^{AA}). GFP-MPS1^{AA} and GFP-MPS1^{DD} mutant proteins were then analyzed for their ability to initiate and sustain SAC signaling alongside WT (GFP-MPS1^{WT}) and kinase-dead (D664A, GFP-MPS1^{KD}) MPS1.

When endogenous MPS1 was replaced with the different forms of GFP-MPS1, GFP-MPS1^{KD} and GFP-MPS1^{AA} showed increased kinetochore levels in comparison to the WT protein (Fig. 3, A, B, and G), indicative of reduced or absent kinase activity (Hewitt et al., 2010; Jelluma et al., 2010; Santaguida et al., 2010). In contrast, GFP-MPS1^{DD} exhibited decreased levels of kinetochore recruitment (Fig. 3, A, B, and G), consistent with the idea that it is constitutively active. Only induction of GFP-MPS1^{WT} or GFP-MPS1^{DD} resulted in the effective recruitment of BUBR1 to the kinetochore and supported a cell cycle arrest in response to nocodazole (Fig. 3, A, C, and D). Taken together, these data suggest that GFP-MPS1^{DD} represents an active form of MPS1.

Consistent with this, purified FLAG-MPS1^{WT} and FLAG-MPS1^{DD} both exhibited a significant phosphorylation-induced band upshift in Western blots that was not observed with kinase activity-deficient FLAG-MPS1^{KD} and FLAG-MPS1^{AA} (Fig. 3 E). FLAG-MPS1^{DD} was less strongly upshifted than FLAG-MPS1^{WT},

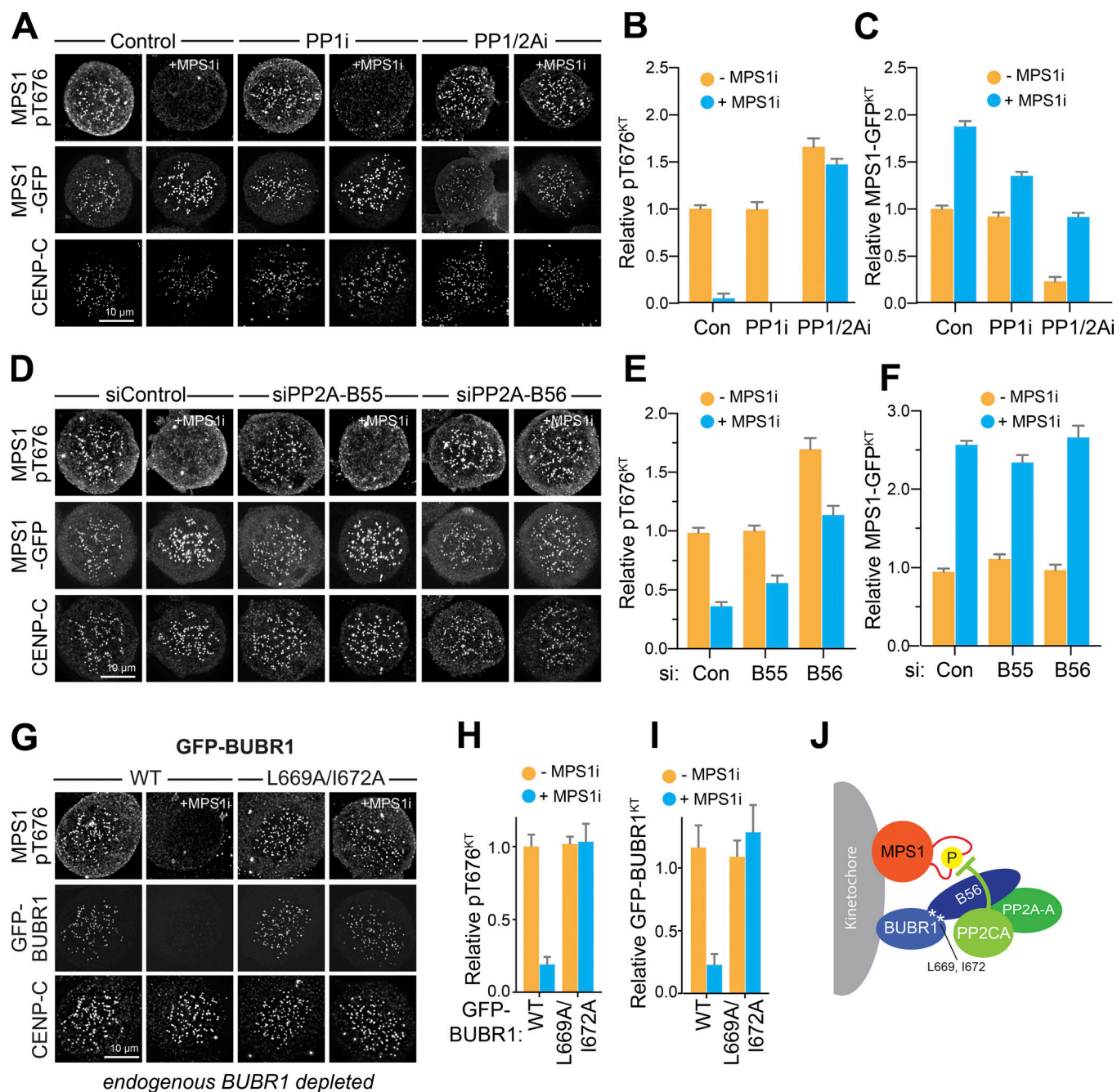


Figure 1. BUBR1-bound PP2A-B56 dephosphorylates MPS1 auto-activatory site T676. (A) Mitotic HeLa MPS1-GFP cells were pretreated with DMSO (Control [Con]), 5 μ M tautomycin (PP1i), or 25 nM calyculin (PP1/PP2Ai), and then 2 μ M MPS1i was added for 5 min where indicated (+MPS1i). MPS1 pT676 and CENP-C were detected using antibodies and total MPS1 by GFP fluorescence. (B and C) Mean kinetochore levels \pm SEM of MPS1 pT676 (B) and MPS1-GFP (C) relative to the -MPS1i control are plotted. (D) MPS1 pT676 phosphorylation and MPS1-GFP localization in control or PP2A-B55- or PP2A-B56-depleted mitotically arrested HeLa MPS1-GFP cells treated with 2 μ M MPS1i. MPS1 pT676 and CENP-C were detected using antibodies, and MPS1 by GFP fluorescence. (E and F) Mean kinetochore levels \pm SEM of MPS1 pT676 (E) and total MPS1-GFP (F) are plotted. (G) HeLa-Flp-In/TREx GFP-BUBR1^{WT} or GFP-BUBR1^{L669A/I672A}-expressing cells depleted of endogenous BUBR1 were mitotically arrested and treated with DMSO (Control) or 2 μ M MPS1i for 5 min. MPS1 pT676 and CENP-C were detected using antibodies, and BUBR1 by GFP fluorescence. (H and I) MPS1 pT676 phosphorylation (H) and mean GFP-BUBR1 kinetochore levels (I) \pm SEM are plotted. (J) Model illustrating how BUBR1-associated PP2A-B56 regulates MPS1 T-loop phosphorylation.

indicating that MPS1^{DD}, although active, had reduced auto-phosphorylation activity in comparison to WT MPS1 (Fig. 3 E). In radioactive kinase assays, FLAG-MPS1^{DD} had $42.60 \pm 7.57\%$ of the kinase activity of WT MPS1, in contrast to $0.72 \pm 0.02\%$ for FLAG-MPS1^{KD} and $16.92 \pm 6.01\%$ for FLAG-MPS1^{AA} (all

normalized to the number of maximally available phosphorylation sites; Tyler et al., 2009; Dou et al., 2011). Despite the somewhat reduced level of autophosphorylation, FLAG-MPS1^{DD} reproducibly phosphorylated a KNL1 fragment in vitro to WT levels (Fig. 3 F), and in all functional assays,

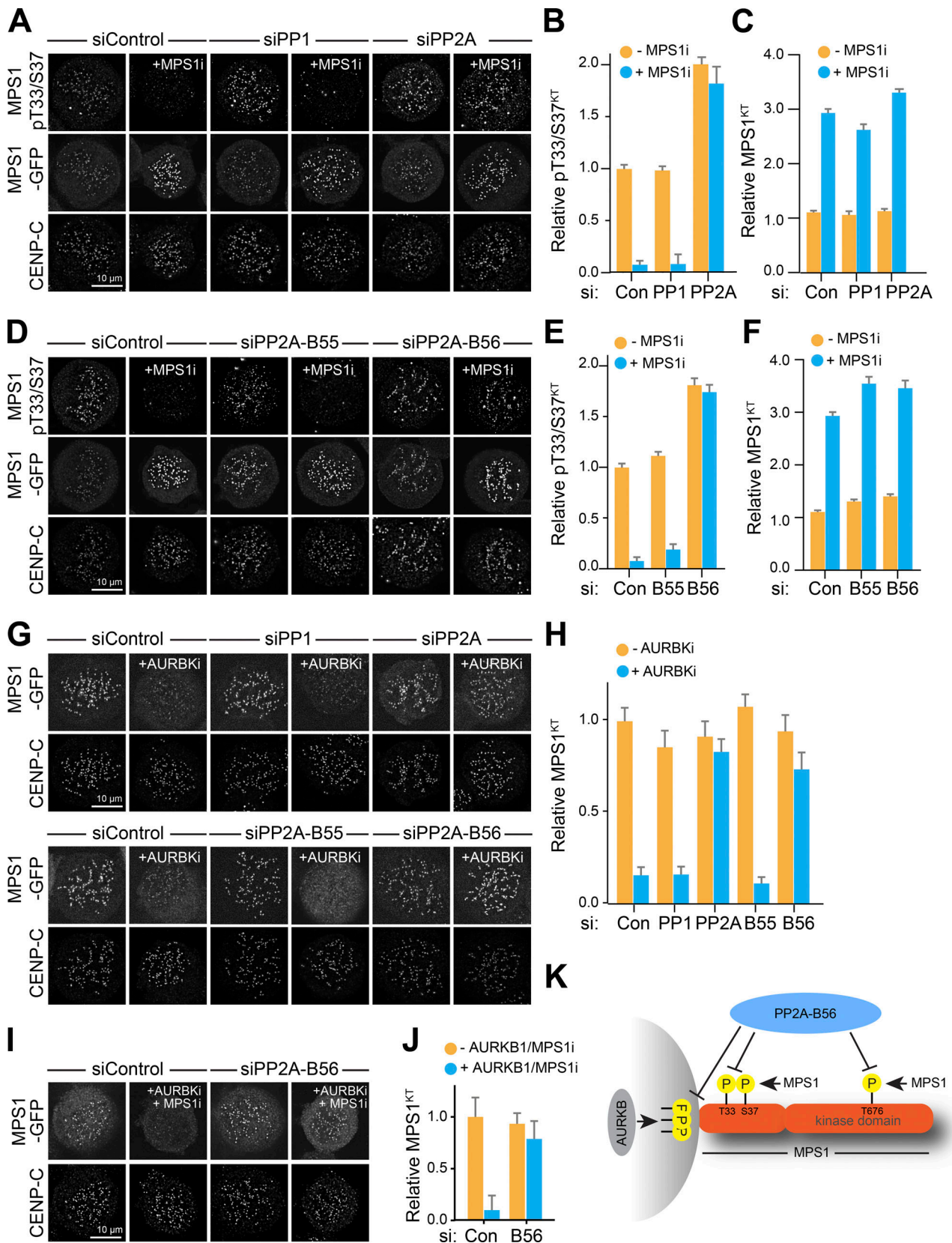


Figure 2. PP2A-B56 modulates MPS1 kinetochore localization by opposing both MPS1 and Aurora B. (A) MPS1 pT33/S37 phosphorylation and MPS1-GFP and CENP-C localization were compared before and after MPS1i (2 μ M) in control, PP1 $\alpha\beta\gamma$, or PP2A catalytic α subunit-depleted HeLa MPS1-GFP cells. (B and C) Mean kinetochore levels \pm SEM of pT33/S37 (B) and total MPS1-GFP (C) relative to CENP-C are plotted. (D) MPS1 pT33/S37 phosphorylation and MPS1-GFP localization were detected in control, PP2A-B55-, or PP2A-B56-depleted cells. (E and F) Mean pT33/S37 (E) and total MPS1-GFP (F) kinetochore

levels \pm SEM relative to CENP-C are plotted. **(G)** MPS1-GFP and CENP-C localization before and after 10-min treatment with 2 μ M AURBK1 in HeLa MPS1-GFP cells (control, PP1 α β γ , PP2A catalytic subunit α , or PP2A-B55 or PP2A-B56 regulatory subunit depleted). **(H)** Mean kinetochore levels \pm SEM of MPS1-GFP relative to CENP-C were plotted. **(I)** MPS1-GFP localization in control depleted or PP2A-B56 depleted HeLa MPS1-GFP cells treated with DMSO or a combination of AURKB1 (2 μ M) and MPS1i (2 μ M) for 10 min. **(J)** Mean kinetochore levels \pm SEM of MPS1-GFP relative to CENP-C were plotted. **(K)** Schematic drawing illustrating kinase and phosphatase regulation of key sites on MPS1 and the kinetochore.

MPS1^{DD} kinase activity appeared to be sufficient to confer WT levels of SAC proficiency (Fig. 3, A–D and G). In summary, these data suggest that MPS1^{DD} can be used to study the consequences of constitutive MPS1 activity.

Unregulated MPS1 activity traps cells in mitosis

To test the consequences of unregulated MPS1 activity for mitotic progression, HeLa-Flp-In/TREx cells depleted of endogenous MPS1 and expressing the different versions of GFP-MPS1 were filmed progressing through mitosis (Fig. 4, A and B). Replacement of endogenous MPS1 with GFP-MPS1^{WT} reinstated normal chromosome segregation and mitotic timing (Fig. 4, A [top] and C–E). Expression of either GFP-MPS1^{KD} or GFP-MPS1^{AA} resulted in onset of chromosome segregation before completion of chromosome alignment and significantly shortened mitotic duration, consistent with a previous report (Jelluma et al., 2008a). These effects were more pronounced for GFP-MPS1^{KD} than for GFP-MPS1^{AA}, in line

with the idea that an MPS1–T-loop alanine mutation allows some residual kinase activity to take place (Fig. 4 A, second and third panel from top; and Fig. 4, C–E). Interestingly, cells expressing GFP-MPS1^{DD} showed a phenotype distinct from both WT and KD and T-loop-deficient GFP-MPS1^{AA}. These cells entered mitosis normally but failed to align all their chromosomes and typically never reached a compact metaphase plate. The bulk of the chromosomes accumulated around a broad pseudometaphase, with chromosomes continuously leaving this arrangement. Most of the cells remained trapped in this pseudometaphase state for several hours and eventually performed an abnormal anaphase or underwent apoptosis (Fig. 4, A [bottom] and C–E).

Constitutively active MPS1 results in impaired microtubule–kinetochore attachment formation

In addition to its role in orchestrating the SAC, MPS1 has been reported to be an important modulator of microtubule–kinetochore

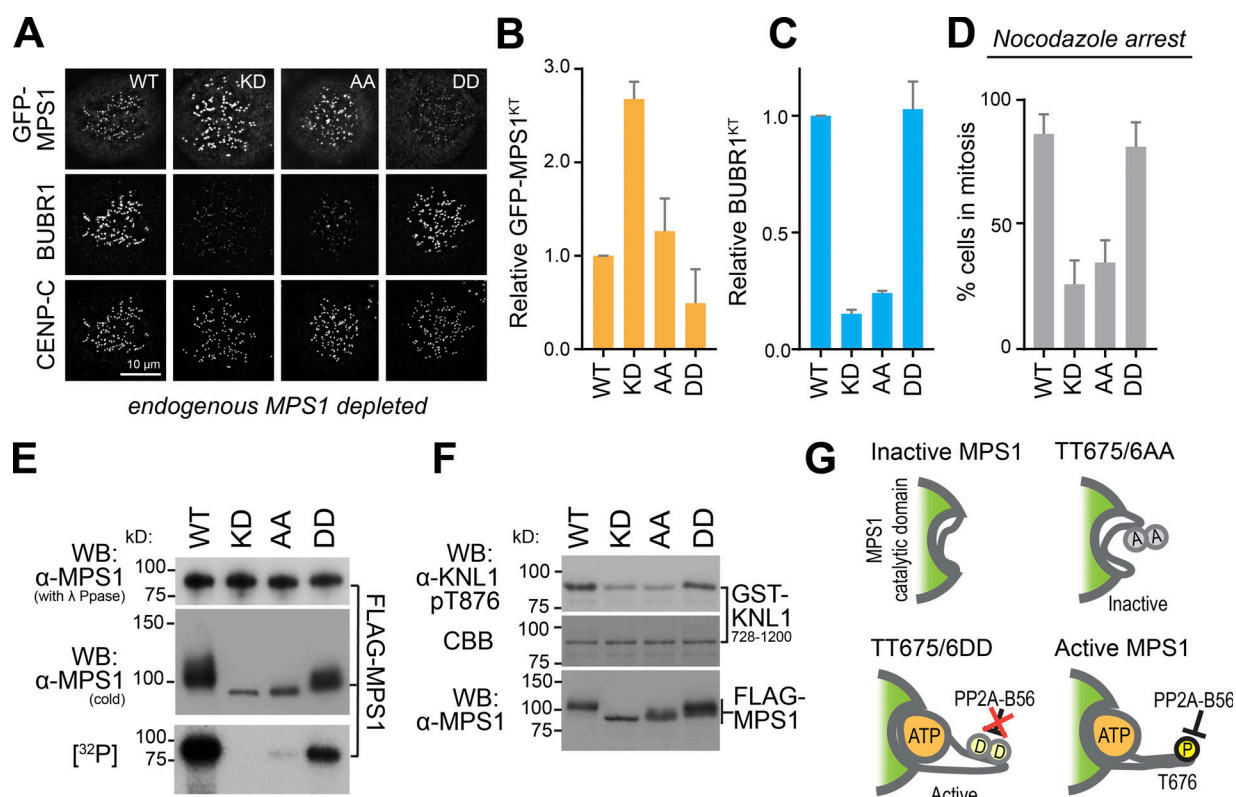


Figure 3. Replacing MPS1 T675 and T676 with aspartic acids restores MPS1 kinase activity and checkpoint functionality. **(A)** GFP-MPS1^{WT}, MPS1^{KD}, MPS1^{AA}, or MPS1^{DD} cells were arrested in mitosis. BUBR1 and CENP-C were detected using antibodies, and MPS1 by GFP fluorescence. **(B and C)** Bar graphs show mean kinetochore-associated GFP-MPS1 (B) and BUBR1 (C) \pm SEM. **(D)** The mean mitotic index \pm SEM of GFP-MPS1^{WT} ($n = 2,490$ cells), MPS1^{KD} ($n = 2,451$ cells), MPS1^{AA} ($n = 2,689$ cells), or MPS1^{DD} ($n = 3,211$ cells) cells after 16-h treatment with 0.33 μ M nocodazole is shown. **(E)** MPS1 autophosphorylation was measured by Western blotting and ³²P incorporation. Equal loading of the different MPS1 forms was confirmed by Western blotting of λ -phosphatase-treated proteins. **(F)** Phosphorylation of GST-KNL1^{728–1,200} by FLAG-MPS1 proteins was assessed by Western blotting with anti-KNL1^{pT875}. Equal loading was confirmed by anti-MPS1 Western blotting. **(G)** Cartoon illustrating how MPS1 TT675/6 mutations affect MPS1 activity.

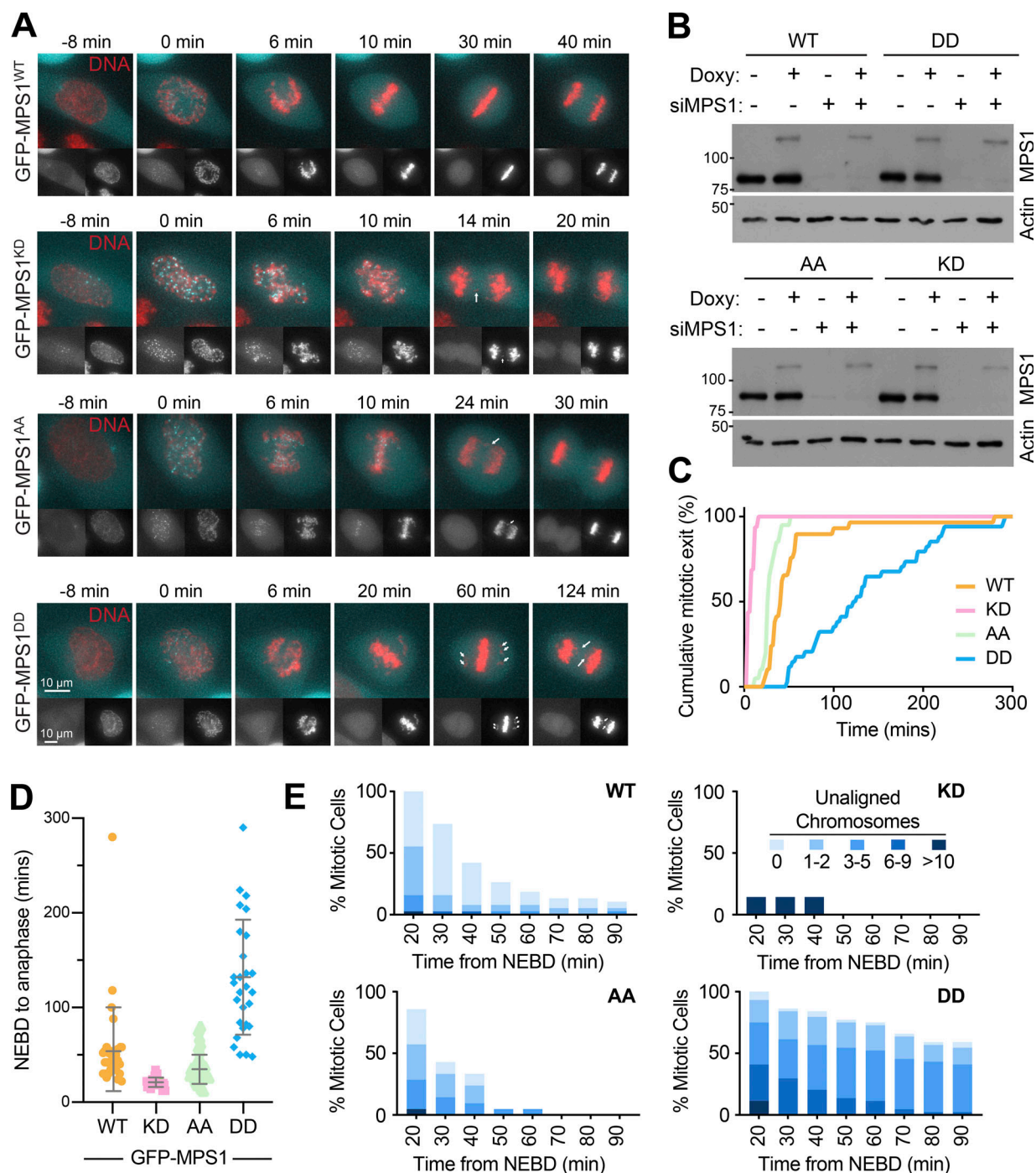


Figure 4. Expression of constitutively active MPS1 (TT675/6DD) results in extended mitotic duration. (A) Cells expressing GFP-MPS1 variants as indicated were filmed passing through mitosis. GFP-MPS1 (cyan and lefthand insert) and DNA (red and righthand insert) are shown. 0 min, nuclear envelope breakdown (NEBD). Anaphase DNA bridges and unaligned chromosomes are indicated by arrows and arrowheads, respectively. See also Videos 1, 2, 3, and 4, showing cells expressing the different GFP-MPS1 mutants progressing through the cell cycle. **(B)** Cell lysates from cells in A were Western blotted for MPS1 and actin (loading control). **(C–E)** Cumulative mitotic exit (C), nuclear envelope breakdown–anaphase duration (D), and proportion of mitotic cells with unaligned chromosomes (E) were plotted over time. In D, each point represents an individual cell with mean \pm SD. Nuclear envelope breakdown–anaphase time shown as bars. Data are from two independent experiments with 35 (WT), 27 (KD), 42 (AA), and 28 (DD) cells measured.

attachments (Jelluma et al., 2008b; Santaguida et al., 2010; Maciejowski et al., 2017). To investigate this role for MPS1, the alignment status of the chromosomes and checkpoint status of the kinetochores was evaluated in GFP-MPS1^{WT} or GFP-MPS1^{DD} cells arrested in mitosis by MG132 treatment. GFP-

MPS1^{DD} cells exhibited significantly more unaligned chromosomes than GFP-MPS1^{WT} cells (Fig. 5, A–C), suggesting that microtubule–kinetochore attachments were compromised. However, once formed, microtubule–kinetochore attachments in MPS1^{DD} cells acquired kinastrin/SKAP staining like

WT cells, indicating that stable attachments could in principle be made (Fig. S3 A; Schmidt et al., 2010). Interestingly, only unattached kinetochores were decorated by GFP-MPS1^{DD} or MAD1 (Fig. 5 C), showing that the behavior of the SAC was not altered by the expression of the constitutively active form of MPS1 per se. To analyze error correction proficiency in more detail, a Monastrol washout assay was employed (Jelluma et al., 2008b). This analysis showed that unregulatable MPS1^{DD}, like kinase-inhibited MPS1, was defective in chromosome alignment upon Monastrol washout. MPS1^{DD}, MPS1^{AA}, and MPS1^{WT} plus MPS1i exhibited significantly fewer aligned metaphase plates than MPS1^{WT} ($P < 0.05$ [DD and AA]; $P < 0.005$ [MPS1i]; Student's *t* test), and MPS1^{DD} exhibited significantly fewer aligned metaphase plates than MPS1^{AA} ($P < 0.05$; Student's *t* test; Fig. 5, D–F). The severity of the phenotype was more pronounced in the complete absence of MPS1 activity than in the unregulatable GFP-MPS1^{DD} mutant, due to the different biological causes underlying the phenotype: in cells treated with MPS1i, the main cause of chromosome alignment defects is the absence of MPS1-dependent recruitment of the BUBR1-bound pool of PP2A-B56 to the kinetochore. Since this pool of PP2A-B56 opposes the error correction activities of both MPS1 and Aurora B (Suijkerbuijk et al., 2012; Kruse et al., 2013; Xu et al., 2013; Maciejowski et al., 2017), this results in unrestrained error correction and a complete failure to align chromosomes upon washout from a Monastrol release (Fig. S3, B and C). In contrast, cells expressing GFP-MPS1^{DD} are proficient in PP2A-B56 recruitment. However, because of the unchecked GFP-MPS1^{DD} kinase activity, the phosphorylation–dephosphorylation balance of MPS1 targets in the error correction process is shifted toward phosphorylation and thus destabilization of attachments. Indeed, phosphorylation of the known MPS1 error correction substrate Ska3 was significantly increased in GFP-MPS1^{DD} cells (Maciejowski et al., 2017; Fig. S3, D and E). In contrast, phosphorylation of Aurora B targets, such as HEC1-Ser55, was unaffected in this situation (Fig. S3, F and G).

To demonstrate that the attachments that are formed in cells expressing GFP-MPS1^{DD} are less well stabilized than in control cells, the interkinetochore distances at aligned and unaligned chromosomes were measured in GFP-MPS1^{WT} and GFP-MPS1^{DD} cells. The KNL1-KNL1 distances at aligned kinetochores in GFP-MPS1^{DD} cells was significantly smaller by 0.233 μm ($P < 0.0001$, Student's *t* test) than in control cells, consistent with a reduction in pulling forces due to decreased microtubule–kinetochore attachment stability (Fig. 5 G).

To further test the idea that cells expressing GFP-MPS1^{DD} excessively turn over microtubule–kinetochore attachments, GFP-MPS1^{DD} and GFP-MPS1^{WT} cells were cold treated to selectively destabilize microtubules not attached to kinetochores. GFP-MPS1^{DD} cells exhibited significantly fewer aligned metaphase plates ($P < 0.05$, Student's *t* test) and fewer cold-stable microtubules ($P < 0.001$, Student's *t* test), confirming an impaired ability to stabilize microtubule–kinetochore attachments (Fig. 5 H). Taken together, the phenotype of the GFP-MPS1^{DD}-expressing cells therefore seems to be primarily a consequence of uncontrolled MPS1-mediated error correction activity rather than unrestrained SAC activity (Jelluma et al., 2008b; Maciejowski et al., 2017).

Human MPS1 has two known functions in the regulation of mitosis: it is the key regulator of the SAC, and together with Aurora B it is actively involved in error correction (Santaguida et al., 2010; Pachis and Kops, 2018). We find here that unregulated kinase activity of MPS1 has a greater effect on error correction than on SAC control. One in-built safeguarding mechanism that mitigates the consequences of hyperactive MPS1 is the fact that MPS1 activity is negatively correlated with its residence time at the kinetochore (Hewitt et al., 2010; Jelluma et al., 2010). A hyperactive MPS1 would therefore be located less well to unattached kinetochores, the critical place for the initiation of spindle checkpoint signaling. Consistent with this idea, we find that the phosphomimetic GFP-MPS1^{DD} mutant shows significantly reduced kinetochore levels in comparison to WT MPS1. The reduced MPS1 kinetochore residence time does not seem to affect spindle checkpoint signaling qualitatively, as cells expressing only GFP-MPS1^{DD} do not have any defects in initializing or maintaining a spindle checkpoint signal (Fig. 3, A–D), although it should be noted that a fraction of GFP-MPS1^{DD} cells eventually exit mitosis in the presence of lagging chromosomes (Fig. 4 A), suggestive of some SAC impairment. More prominently though, GFP-MPS1^{DD} cells do show signs of exaggerated error correction, apparent as the inability to align all chromosomes to a metaphase plate, reduced interkinetochore distances of aligned chromosomes, and diminished numbers of cold-stable K-fibers (Fig. 5). These observations are in line with the idea that MPS1 phosphorylates outer kinetochore targets, including the Ska complex, to destabilize erroneous attachments (Maciejowski et al., 2017).

PP2A-B56 has been shown to counteract the microtubule–kinetochore attachment destabilizing activities of MPS1 as well as Aurora B (Foley et al., 2011; Suijkerbuijk et al., 2012; Kruse et al., 2013; Xu et al., 2013; Maciejowski et al., 2017). Using the same phosphatase to oppose both kinases thus allows coordinated stabilization of microtubule–kinetochore attachments. Our data indicate that PP2A-B56 not only dephosphorylates important targets of MPS1 in the error correction pathway but also controls key regulatory residues on MPS1 itself. Intriguingly, in *Drosophila*, this latter function of dephosphorylating the MPS1 T-loop is performed by PPI, not PP2A-B56, and seems to mainly affect MPS1's role in controlling the SAC and not error correction, as *Drosophila* cells depleted of PPI did not show any signs of elevated error correction (Moura et al., 2017). The reason for this difference from human cells may be found in the distinct wiring of some aspects of the SAC in flies in comparison to human cells. Most relevant for this discussion, it is not clear whether *Drosophila* has a distinct kinetochore pool of PP2A-B56. Certain functionalities of PP2A-B56 may therefore be performed by PPI in flies. In human cells, PP2A-B56 emerges as the principal phosphatase opposing MPS1 phosphorylation events throughout mitosis, and our data further highlight the importance of this regulation.

Materials and methods

Reagents and antibodies

General laboratory chemicals and reagents were obtained from Sigma-Aldrich and Thermo Fisher Scientific unless specifically

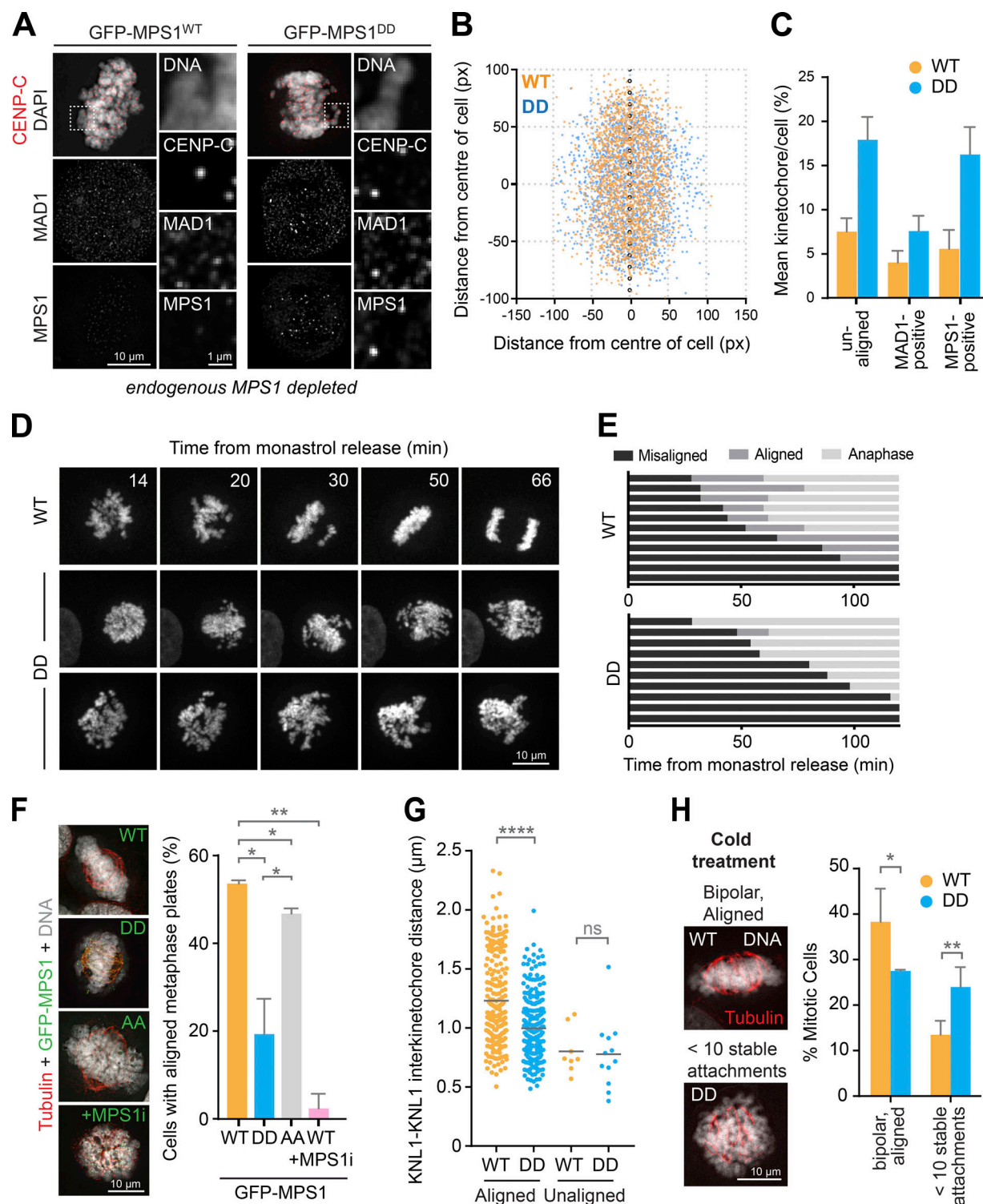


Figure 5. Microtubule-kinetochore interactions are perturbed in the presence of constitutively active MPS1. (A) MPS1^{WT} or GFP-MPS1^{DD} mitotic cells were stained for DNA (gray), MAD1, and CENP-C (red in the merged image). MPS1 was visualized by GFP fluorescence. An enlarged image of kinetochore pairs (attached in WT, one unattached in DD), indicated by a dashed box, is shown on the righthand side of the images. (B and C) The x-y distance of individual kinetochores from the cell center in 23 (MPS1^{WT}) or 19 (MPS1^{DD}) cells (B) and the proportion of misaligned, MAD1-positive or MPS1-positive kinetochores were plotted (C; mean \pm SEM). (D and E) GFP-MPS1^{WT} or MPS1^{DD} cells were filmed after Monastrol washout (D), and the fate of individual cells was tracked (E). Each horizontal bar represents a single cell. (F) GFP-MPS1 cells were released from Monastrol arrest into MG132 for 60 min in the presence or absence of 2 μ M MPS1i. DNA (gray), microtubules (red), and GFP-MPS1 (green) are shown. Mean proportion \pm SD of cells exhibiting aligned metaphase plates is plotted in the bar graphs. (G) KNL1-KNL1 interkinetochore distance is shown in GFP-MPS1^{WT} or GFP-MPS1^{DD} cells treated as in A. Each dot represents a kinetochore pair, and the gray bar represents the mean of 234 (WT) and 290 (DD) kinetochore pairs across 19 cells per condition from two independent experiments. ns, not significant ($P > 0.05$); *, $P \leq 0.05$; **, $P \leq 0.001$; ****, $P \leq 0.0001$. (H) Cells as in A were cold treated before fixation. DNA is shown in gray and microtubules in red. The mean proportions \pm SD of cells (282 WT and 331 DD cells from three independent experiments) with aligned metaphase plates or <10 stable microtubule-kinetochore attachments are plotted.

indicated. Inhibitors were obtained from Tocris Bioscience (MPS1-inhibitor AZ3146, 20 mM stock; PP1 and PP2A inhibitors calyculin A, 1 mM stock; PP1 inhibitor tautomycin, 2.5 mM stock), Insight Bioscience (proteasome inhibitor MG132, 20 mM stock), Merck (microtubule polymerization inhibitor nocodazole, 6 mM stock), and Cambridge Bioscience (Eg5 inhibitor Monastrol, 100 mM stock). Inhibitor stocks were prepared in DMSO. Thymidine (Sigma-Aldrich; 100 mM stock) and doxycycline (InvivoGen; 2 mM stock) were dissolved in water. DNA vital dye SiR-Hoechst (Spirochrome) was dissolved in DMSO and used at 50 nM final concentration.

Commercially available mAbs or polyclonal antibodies (pAbs) were used for MAD1 (rabbit pAb; Genetex; GTX105079), BUBR1 (rabbit pAb; Bethyl; A33-386A), β -actin (HRP conjugated; mouse mAb; Abcam; [AC-15] ab49900), Tubulin (mouse mAb; Sigma-Aldrich; [DM1A] T6199), PPP1CA (rabbit pAb; Bethyl; A300-904A), PPP1CC (goat pAb; Santa Cruz; sc6108), PP2CA (goat pAb; Santa Cruz; SC6112), PP4C (rabbit pAb; Bethyl; A300-835A), PP5C (rabbit pAb; Bethyl; A300-909A), PP6C (rabbit pAb; Bethyl; A300-844A), PPP2R2A (mouse mAb; Cell Signaling; [2G9] 5689S), PPP2R5A (rabbit pAb; Bethyl; A300-967A), PPP2R5D (mouse mAb; Millipore; [H5D12] 04-639), PPP2R5E (mouse mAb; Santa Cruz; [A-11] sc-376176), phospho-MPS1T33/S37 (pRb; Thermo Fisher Scientific; 44-1325G), centromere protein C (CENP-C; guinea pig pAb; MBL; PDO30), FLAG epitope tag (mouse mAb; Thermo Fisher Scientific; [FG4R] MA1-91878), and GFP (rabbit pAb; Abcam; ab290). Human CREST serum was obtained from Antibodies Inc. (15-234-0001). Sheep antibodies against kinastrin have been described previously (Dunsch et al., 2011). Antibodies against MPS1 were raised in sheep (Scottish Blood Transfusion Services) against recombinant His-tagged MPS1 (amino acids 1-260) and affinity purified against the same recombinant protein. Antibodies to MPS1 phosphorylated at T676 were raised in sheep (Scottish Blood Transfusion Services) and affinity purified using the peptide sequence CMQPDT(pT)SVVKDS. Antibodies to HEC1-pSer55 were raised in sheep (Orygen) and purified using the peptide sequence CSERKV(pS)LFGKR. Antibodies to Ska3-pSer34 (Maciejowski et al., 2017) were a generous gift from Prasad Jallepalli. Generation of anti-KNL1^{PT875} has been described previously (Espert et al., 2014). Secondary donkey antibodies against mouse, rabbit, guinea pig, or sheep, labeled with Alexa Fluor 488, 555, or 647; Cy5; or HRP were purchased from Molecular Probes and Jackson ImmunoResearch Laboratories. Affinity-purified primary and HRP-coupled secondary antibodies were used at 1 μ g/ml final concentration. For Western blotting, proteins were separated by SDS-PAGE and transferred to nitrocellulose using a Trans-blot Turbo system (Bio-Rad). Protein concentrations were measured by Bradford assay using Protein Assay Dye Reagent Concentrate (Bio-Rad). All Western blots were revealed using ECL (GE Healthcare).

Molecular biology

Human MPS1 was amplified from human testis cDNA (Marathon cDNA; Takara Bio) using Pfu polymerase (Agilent Technologies). MPS1 expression constructs were made using pcDNA5/FRT/TO vectors (Invitrogen) modified to encode the EGFP or FLAG

reading frames. Mutagenesis was performed using the Quik-Change method (Agilent Technologies). DNA primers were obtained from Invitrogen. siRNA duplexes targeting PPP family phosphatase subunits BUBR1 and MPS1 have been described previously (Zeng et al., 2010; Espert et al., 2014; Hayward et al., 2019). On-target SMARTPools were obtained from Dharmacon Horizon.

Cell culture procedures

HeLa cells and HEK293T were cultured in DMEM and hTert-RPE-1 cells in DMEM/F12 medium, all with 1% (vol/vol) Gluta-MAX (Life Technologies) and containing 10% (vol/vol) bovine calf serum, at 37°C and 5% CO₂. For plasmid transfection and siRNA transfection, Mirus LT1 (Mirus Bio) and Oligofectamine (Invitrogen), respectively, were used. HeLa cell lines with single integrated copies of the desired transgene were created using the T-Rex doxycycline-inducible Flp-In system (Invitrogen; Tighe et al., 2004). CRISPR/Cas9-edited HeLa cells with an inserted GFP tag in the C-terminus of the TTK/MPS1 gene product and HeLa cells stably expressing GFP-MAD2 have been described previously (Alfonso-Pérez et al., 2019; Hayward et al., 2019).

RNAi rescue assays

MPS1 siRNA rescue was performed by induction of GFP-MPS1 transgene for 6 h before a 48-h siRNA depletion of endogenous MPS1 using oligonucleotides against the 3' UTR (5'-UUGGAC UGUUAUACUCUUGAA-3', 5'-GUGGAUAGCAAGUAUUAUCUA-3', and 5'-CUUGAAUCCUGUGGAAAU-3'; Hayward et al., 2019). A second induction was performed 24 h into the siRNA depletion. GFP-BubR1 was induced 6 h before a 48-h siRNA depletion of endogenous BubR1 using oligonucleotides against the 3' UTR (5'-GCAATCAAGTCTCACAGAT-3'; Espert et al., 2014). A second induction was performed 24 h into the siRNA depletion.

Mitotic arrests and inhibitions

Unless otherwise stated, mitotically arrested cells were generated by addition of nocodazole (0.33 μ M, 2.5 h) followed by MG132 (20 μ M, 0.5 h). Monastrol washouts (Fig. 5, D, E, and F) were performed by adding Monastrol at 100 μ M for 2.5 h, followed by washing cells three times with warm PBS and three times with warm DMEM. In Fig. 5 F, 20 μ M MG132 was added for 60 min after washout. Cold treatment of cells (Fig. 5 H) was performed by incubating cells at 4°C for 9 min before fixation to depolymerize microtubules that had not formed stable K-fibers. Inhibitor vehicle for all drugs was DMSO, and DMSO alone was added as control. A complete list of the inhibitors and targets is found in Table 1.

Immunofluorescence microscopy and image processing

Cells were fixed with PTEMF (20 mM Pipes-KOH, pH 6.8, 0.2% [vol/vol] Triton X-100, 1 mM MgCl₂, 10 mM EGTA, and 4% [wt/vol] formaldehyde; Dunsch et al., 2011) except for pSka3 staining in Fig. S3 D, where cells were fixed with preextraction: 37°C for 90 s in PEMGT (100 mM Pipes, pH 6.9, 10 mM EGTA, 1 mM MgCl₂, 4 M glycerol, and 0.5% Triton X-100) followed by a 10-min fixation in PEMGT plus 3.7% formaldehyde, 0.2% Triton

Table 1. Mitotic inhibition materials

Inhibitor target	Inhibitor	Acronym used in text	Drug concentration	Time of drug addition before fixation (min)
MPS1	AZ3145	MPS1i	2 μ M	5
PP1	Tautomycin	PP1i	5 μ M	30
PP1 and PP2A	Calyculin A	PP1/PP2Ai	25 nM	6
Aurora B	ZM447439	AURBK1	2 μ M	10

X-100, and 1 μ M calyculin A. For pHEC1 staining (Fig. S3 F), 1 μ M calyculin A was included during PTEMF fixation. Antibody dilutions were performed in PBS with 3% (wt/vol) BSA. Samples seeded on #1 thickness coverslips were imaged on a DeltaVision Core light microscopy system (GE Healthcare) using either a 60 \times /1.35-NA or 100 \times /1.4-NA objective fitted to an Olympus IX-71 microscope stand. Standard filter sets for DAPI (excitation 390/18, emission 435/48), FITC (excitation 475/28, emission 525/48), TRITC (excitation 542/27, emission 597/45), and Cy-5 (excitation 632/22, emission 676/34) were used to sequentially excite and collect fluorescence images on a CoolSnap HQ2 CCD camera (Photometrics) using the software package softWoRx (GE Healthcare). Cells were imaged using a 0.2- μ m interval and a total stack of 2 μ m and deconvolved for presentation using softWoRx. Image stacks were imported into Fiji (Schindelin et al., 2012) for maximum-intensity projection and saved as 8-bit TIFF files. TIFF files were imported into Illustrator CS6 (Adobe) for figure production. For quantification, imaging was performed using a 60 \times /1.35-NA oil-immersion objective on a BX61 Olympus microscope equipped with filter sets for DAPI, EGFP/Alexa Fluor 488, 555, and 647 (Chroma Technology Corp.), a CoolSNAP HQ2 camera (Roper Scientific), and MetaMorph 7.5 imaging software (GE Healthcare).

Quantification and statistical analysis

Image analysis was performed in Fiji and Excel (Microsoft). 10 Z-stacks with a 0.2- μ m interval were sum projected for analysis. Relative protein kinetochore intensities (Fig. 1, B, C, E, F, H, and I; Fig. 2, B, C, E, F, H, and J; Fig. 3, B and C; Fig. S1, D, E, G, and H; Fig. S2 E; and Fig. S3, E and G) were determined by placing a 10-pixel-wide circular region of interest over individual kinetochores and measuring the mean pixel fluorescence, before dividing by the mean pixel intensity of the CENP-C channel within the same ROI. A mean background (cytoplasm) intensity for each cell is subtracted from each kinetochore protein or CENP-C measurement. The mean protein fluorescence of each kinetochore was divided by the mean kinetochore intensity of the total control population (always the condition closest to the y axis, with a value of 1) to generate relative values, which were plotted as bar graphs. For all immunofluorescence experiments, >15 cells per condition were analyzed with \geq 10 kinetochores per cell. All immunofluorescence experiments shown are representative of at least two independent experiments pooled together. Unless otherwise stated, error bars represent the SEM, with *n* as the number of cells measured. Production of graphs was performed on Prism (GraphPad

Software) using data exported from Excel. Statistical analysis of kinetochore intensities was performed in Excel or Prism.

Interkinetochore distance

KNL1-KNL1 interkinetochore distance measurements were taken in a 3D space from 234 (WT) and 290 (DD) kinetochore pairs across 19 cells per condition from two independent experiments. Distances between a kinetochore pair are plotted as individual points, with the mean distance plotted as a black bar. Student's *t* test was performed to determine statistical significance.

Kinetochore positioning measurements

Kinetochore positions were identified as the center of mass of CENP-C signals identified within the cell boundary following equal thresholding of images and were plotted in Fig. 5 B by distance in pixels from the center of the cell. 23 (WT) or 19 (DD) randomly selected cells were measured. There was no significant difference (Student's *t* test) between the number of identified kinetochores per cell in WT (mean 91, SD 17) and DD (mean 94, SD 15). The alignment status of these kinetochores in Fig. 5 C was determined as defining aligned kinetochores as being positioned within the 50% region of the x axis closest to the center of a cell (i.e., within 25% either side of the center of the cell along the x axis). Misaligned kinetochores are therefore defined as being outside of this zone. Proportion of MAD1- and MPS1-positive kinetochores were quantified as the number of objects within the cell boundary counted after equal thresholding of image channels.

Live-cell microscopy and statistical analysis

Time-lapse imaging of cells with a paired control sample was performed on a DeltaVision Elite light microscopy system as described for fixed cell samples. Fluorescence images were collected on a 512 \times 512-pixel electron-multiplying charge-coupled device camera (QuantEM; Photometrics) using the software package softWoRx (GE Healthcare). Cells were placed in a 37°C and 5% CO₂ environmental chamber (Tokai Hit) on the microscope stage with lens heating collar. Cells were seeded on two-chambered glass-bottom dishes (Lab-Tek) at 30,000 per well. SiR-Hoechst was added 8 h before imaging at a final concentration of 100 nM. Typically, seven planes were captured per cell 2 μ m apart every 2 min, with laser powers at 2% and 25-ms exposures. Deconvolution and maximum-intensity projections were performed using softWoRx, with image cropping performed using Fiji.

All other time-lapse imaging was performed using an Ultra-view Vox spinning disc confocal system (PerkinElmer) mounted

on an Olympus IX81 inverted microscope, a 512 × 512-pixel electron-multiplying charge-coupled device camera (ImagEM C9100-13; Hamamatsu Photonics), and Velocity software. Cells were placed in a 37°C and 5% CO₂ environmental chamber on the microscope stage with lens heating collar. Imaging was performed using a 60× 1.4-NA oil-immersion objective, 4–12% laser power, and 30–200-ms exposure time. Typically, 19 planes 0.6 μm apart were imaged every 2 min. Maximum-intensity projection or summed projection of the fluorescent channels was performed in Fiji. Statistical analysis of live-cell imaging data (Figs. 2 C and 4 D) was performed in GraphPad Prism.

Protein expression and purification

FLAG-MPS1^{WT}, FLAG-MPS1^{KD}, FLAG-MPS1^{AA}, and FLAG-MPS1^{DD} were expressed and purified from HEK293T cells. For each construct, two 15-cm dishes of cells were transfected with 8 μg DNA, each, for 36 h, including a 12-h nocodazole arrest. Cell pellets were lysed in 1 ml lysis buffer (20 mM Tris-HCl, pH 7.4, 300 mM NaCl, 1% [vol/vol] Triton X-100, and protease inhibitor cocktail [Sigma-Aldrich]). MPS1 was immunoprecipitated from the clarified supernatants using 100 μl FLAG-agarose beads (Sigma-Aldrich). Immunoprecipitates were washed twice with lysis buffer; four times with 20 mM Tris-HCl, pH 7.4, 300 mM NaCl, and 0.1% [vol/vol] Triton X-100; two times with 20 mM Tris-HCl, pH 7.4, and 300 mM NaCl; and once with 100 mM Tris-HCl, pH 7.4. GST-tagged KNL1^{728–1,200} was expressed and purified as described previously (Espert et al., 2014). Purification of insect cell-expressed His-MPS1 has previously been described (Espert et al., 2014).

MPS1 kinase assays

For kinase assays, 1 μg recombinant GST-Knl1^{728–1,200} was phosphorylated with 1 μg recombinant FLAG-MPS1 on FLAG-agarose beads for 30 min at 30°C in 50 mM Tris-HCl, pH 7.3, 50 mM KCl, 10 mM MgCl₂, 20 mM sodium β-glycerophosphate, 15 mM EGTA, 0.2 mM (cold assay) or 0.1 mM (hot assay) ATP, 1 mM DTT, and 1 μCi [³²P]γ-ATP (hot assay) per reaction. Incorporation of γ-³²P into MPS1 or pKNL1⁸⁷⁵ intensity was used as a readout of kinase activity. Coomassie-stained bands of FLAG-MPS1 with incorporated γ-³²P on an SDS-PAGE were excised for scintillation counting. The mean proportion ± SD of MPS1 mutant protein activity (counts per minute) relative to WT was determined across two independent experiments. The values were then normalized to the intensity of the Coomassie blue-stained band (measured with ImageJ) and the number of available phosphorylation sites to account for the fact that FLAG-MPS1^{AA} and FLAG-MPS1^{DD} were lacking two sites. These two proteins were considered to have 10 available sites, and FLAG-MPS1^{WT} and FLAG-MPS1^{KD}, 12 sites (Tyler et al., 2009; Dou et al., 2011). For the accurate determination of protein loading by Western blotting, FLAG-MPS1 was dephosphorylated using Lambda Phosphatase (NEB) and 1 mM DTT for 1 h at 30°C.

Online supplemental material

Fig. S1 shows the specificity of the MPS1 pT676 antibody, MPS1-T-loop phosphorylation in RPE-1 cells, and the full phosphatase catalytic subunit RNAi screen for pT676 retention upon MPS1 inhibition, supporting Fig. 1. Fig. S2 shows Western blots demonstrating

phosphatase and BUBR1 depletion as well as BUBR1 transgene induction, and pT676 staining in control or PP1- or PP2A-B56-depleted cells with intact microtubules, supporting Figs. 1 and 2. Fig. S3 shows kinastrin staining in cells expressing GFP-MPS1 WT or DD, error correction assays in cells expressing GFP-BUBR1^{L669A/1672A} and SKA3-pSer34, as well as HEC1-pSer55 phosphorylation in GFP-MPS1^{DD} cells, supporting Fig. 5. Videos 1, 2, 3, and 4 show cells expressing the different GFP-MPS1 mutants progressing through the cell cycle, supplementing Fig. 4.

Acknowledgments

We thank Stephen Taylor (University of Manchester, Manchester, UK) for Hela-Flp-In/TREx cells, Prasad Jallepalli (Memorial Sloan-Kettering Cancer Center, New York, NY) for SKA3 pS34 antibody, Jakob Nilsson (University of Copenhagen, Copenhagen, Denmark) for helpful advice regarding phosphomimetic mutants, Dr. Renaud Caous for HEC1-pSer55 antibody purification, and Iona Manley and Zoë Geraghty for critical reading of the manuscript.

D. Hayward was supported by a Medical Research Council Senior Non-Clinical Research fellowship awarded to U. Gruneberg (MR/K006703/1) and T. Alfonso-Pérez by a Biotechnology and Biological Sciences Research Council Strategic LoLa grant (BB/M00354X/1).

The authors declare no competing financial interests.

Author contributions: Conceptualization: U. Gruneberg. Investigation: D. Hayward, J. Bancroft, T. Alfonso-Pérez, D. Mangat, S. Dugdale, and J. McCarthy. Funding acquisition: U. Gruneberg, F.A. Barr. Supervision: U. Gruneberg, F.A. Barr. Writing – original draft: U. Gruneberg. Writing – review and editing: T. Alfonso-Pérez, D. Hayward, J. Bancroft, F. A. Barr, U. Gruneberg.

Submitted: 5 May 2019

Revised: 19 July 2019

Accepted: 6 August 2019

References

- Alfonso-Pérez, T., D. Hayward, J. Holder, U. Gruneberg, and F.A. Barr. 2019. MAD1-dependent recruitment of CDK1-CCNB1 to kinetochores promotes spindle checkpoint signaling. *J. Cell Biol.* 218:1108–1117. <https://doi.org/10.1083/jcb.201808015>
- Choy, M.S., M. Swingle, B. D'Arcy, K. Abney, S.F. Rusin, A.N. Kettenbach, R. Page, R.E. Honkanen, and W. Peti. 2017. PP1:Tautomycin Complex Reveals a Path toward the Development of PP1-Specific Inhibitors. *J. Am. Chem. Soc.* 139:17703–17706. <https://doi.org/10.1021/jacs.7b09368>
- Ciliberto, A., and S. Hauf. 2017. Micromanaging checkpoint proteins. *eLife*. 6:e25001. <https://doi.org/10.7554/eLife.25001>
- Combes, G., H. Barysz, C. Garand, L. Gama Braga, I. Alharbi, P. Thebault, L. Murakami, D.P. Bryne, S. Stankovic, P.A. Eyers, et al. 2018. Mps1 Phosphorylates Its N-Terminal Extension to Relieve Autoinhibition and Activate the Spindle Assembly Checkpoint. *Curr. Biol.* 28:872–883.e5. <https://doi.org/10.1016/j.cub.2018.02.002>
- Dodson, C.A., T. Haq, S. Yeoh, A.M. Fry, and R. Bayliss. 2013. The structural mechanisms that underpin mitotic kinase activation. *Biochem. Soc. Trans.* 41:1037–1041. <https://doi.org/10.1042/BST20130066>
- Dou, Z., C. von Schubert, R. Körner, A. Santamaria, S. Elowe, and E.A. Nigg. 2011. Quantitative mass spectrometry analysis reveals similar substrate consensus motif for human Mps1 kinase and Plk1. *PLoS One*. 6:e18793. <https://doi.org/10.1371/journal.pone.0018793>

- Dunsch, A.K., E. Linnane, F.A. Barr, and U. Gruneberg. 2011. The astrin-kinastrin/SKAP complex localizes to microtubule plus ends and facilitates chromosome alignment. *J. Cell Biol.* 192:959–968. <https://doi.org/10.1083/jcb.201008023>
- Espert, A., P. Ulucak, R.N. Bastos, D. Mangat, P. Graab, and U. Gruneberg. 2014. PP2A-B56 opposes Mps1 phosphorylation of Knl1 and thereby promotes spindle assembly checkpoint silencing. *J. Cell Biol.* 206: 833–842. <https://doi.org/10.1083/jcb.201406109>
- Faesen, A.C., M. Thanasoula, S. Maffini, C. Breit, F. Müller, S. van Gerwen, T. Bange, and A. Musacchio. 2017. Basis of catalytic assembly of the mitotic checkpoint complex. *Nature.* 542:498–502. <https://doi.org/10.1038/nature21384>
- Foley, E.A., M. Maldonado, and T.M. Kapoor. 2011. Formation of stable attachments between kinetochores and microtubules depends on the B56-PP2A phosphatase. *Nat. Cell Biol.* 13:1265–1271. <https://doi.org/10.1038/ncb2327>
- Hayward, D., T. Alfonso-Pérez, M.J. Cundell, M. Hopkins, J. Holder, J. Bancroft, L.H. Hutter, B. Novak, F.A. Barr, and U. Gruneberg. 2019. CDK1-CENB1 creates a spindle checkpoint-permissive state by enabling MPS1 kinetochore localization. *J. Cell Biol.* 218:1182–1199. <https://doi.org/10.1083/jcb.201808014>
- Hertz, E.P.T., T. Kruse, N.E. Davey, B. López-Méndez, J.O. Sigurdsson, G. Montoya, J.V. Olsen, and J. Nilsson. 2016. A Conserved Motif Provides Binding Specificity to the PP2A-B56 Phosphatase. *Mol. Cell.* 63:686–695. <https://doi.org/10.1016/j.molcel.2016.06.024>
- Hewitt, L., A. Tighe, S. Santaguida, A.M. White, C.D. Jones, A. Musacchio, S. Green, and S.S. Taylor. 2010. Sustained Mps1 activity is required in mitosis to recruit O-Mad2 to the Mad1-C-Mad2 core complex. *J. Cell Biol.* 190:25–34. <https://doi.org/10.1083/jcb.201002133>
- Ishihara, H., B.L. Martin, D.L. Brautigan, H. Karaki, H. Ozaki, Y. Kato, N. Fusetani, S. Watabe, K. Hashimoto, D. Uemura, et al. 1989. Calyculin A and okadaic acid: inhibitors of protein phosphatase activity. *Biochem. Biophys. Res. Commun.* 159:871–877. [https://doi.org/10.1016/0006-291X\(89\)92189-X](https://doi.org/10.1016/0006-291X(89)92189-X)
- Jelluma, N., A.B. Brenkman, I. McLeod, J.R. Yates III, D.W. Cleveland, R.H. Medema, and G.J. Kops. 2008a. Chromosomal instability by inefficient Mps1 auto-activation due to a weakened mitotic checkpoint and lagging chromosomes. *PLoS One.* 3:e2415. <https://doi.org/10.1371/journal.pone.0002415>
- Jelluma, N., A.B. Brenkman, N.J. van den Broek, C.W. Cruikshank, M.H. van Osch, S.M. Lens, R.H. Medema, and G.J. Kops. 2008b. Mps1 phosphorylates Borealin to control Aurora B activity and chromosome alignment. *Cell.* 132:233–246. <https://doi.org/10.1016/j.cell.2007.11.046>
- Jelluma, N., T.B. Dansen, T. Slidrecht, N.P. Kwiatkowski, and G.J. Kops. 2010. Release of Mps1 from kinetochores is crucial for timely anaphase onset. *J. Cell Biol.* 191:281–290. <https://doi.org/10.1083/jcb.201003038>
- Ji, Z., H. Gao, L. Jia, B. Li, and H. Yu. 2017. A sequential multi-target Mps1 phosphorylation cascade promotes spindle checkpoint signaling. *eLife.* 6:e22513. <https://doi.org/10.7554/eLife.22513>
- Kang, J., Y. Chen, Y. Zhao, and H. Yu. 2007. Autophosphorylation-dependent activation of human Mps1 is required for the spindle checkpoint. *Proc. Natl. Acad. Sci. USA.* 104:20232–20237. <https://doi.org/10.1073/pnas.0710519105>
- Kruse, T., G. Zhang, M.S. Larsen, T. Lischetti, W. Streicher, T. Kragh Nielsen, S.P. Bjørn, and J. Nilsson. 2013. Direct binding between BubR1 and B56-PP2A phosphatase complexes regulate mitotic progression. *J. Cell Sci.* 126:1086–1092. <https://doi.org/10.1242/jcs.122481>
- Liu, X., and M. Winey. 2012. The MPS1 family of protein kinases. *Annu. Rev. Biochem.* 81:561–585. <https://doi.org/10.1146/annurev-biochem-061611-090435>
- Maciejowski, J., H. Drechsler, K. Grundner-Culemann, E.R. Ballister, J.A. Rodriguez-Rodriguez, V. Rodriguez-Bravo, M.J.K. Jones, E. Foley, M.A. Lampson, H. Daub, et al. 2017. Mps1 Regulates Kinetochore-Microtubule Attachment Stability via the Ska Complex to Ensure Error-Free Chromosome Segregation. *Dev. Cell.* 41:143–156.e6. <https://doi.org/10.1016/j.devcel.2017.03.025>
- Mattison, C.P., W.M. Old, E. Steiner, B.J. Huneycutt, K.A. Resing, N.G. Ahn, and M. Winey. 2007. Mps1 activation loop autophosphorylation enhances kinase activity. *J. Biol. Chem.* 282:30553–30561. <https://doi.org/10.1074/jbc.M707063200>
- Mitsuhashi, S., N. Matsuura, M. Ubukata, H. Oikawa, H. Shima, and K. Kikuchi. 2001. Tautomycin is a novel and specific inhibitor of serine/threonine protein phosphatase type 1, PP1. *Biochem. Biophys. Res. Commun.* 287:328–331. <https://doi.org/10.1006/bbrc.2001.5596>
- Moura, M., M. Osswald, N. Leça, J. Barbosa, A.J. Pereira, H. Maiato, C.E. Sunkel, and C. Conde. 2017. Protein Phosphatase 1 inactivates Mps1 to ensure efficient Spindle Assembly Checkpoint silencing. *eLife.* 6:e25366. <https://doi.org/10.7554/eLife.25366>
- Musacchio, A. 2015. The Molecular Biology of Spindle Assembly Checkpoint Signaling Dynamics. *Curr. Biol.* 25:R1002–R1018. <https://doi.org/10.1016/j.cub.2015.08.051>
- Nijenhuis, W., E. von Castelmur, D. Littler, V. De Marco, E. Tromer, M. Vleugel, M.H. van Osch, B. Snel, A. Perrakis, and G.J. Kops. 2013. A TPR domain-containing N-terminal module of MPS1 is required for its kinetochore localization by Aurora B. *J. Cell Biol.* 201:217–231. <https://doi.org/10.1083/jcb.201210033>
- Nijenhuis, W., G. Vallardi, A. Teixeira, G.J. Kops, and A.T. Saurin. 2014. Negative feedback at kinetochores underlies a responsive spindle checkpoint signal. *Nat. Cell Biol.* 16:1257–1264. <https://doi.org/10.1038/ncb3065>
- Pachis, S.T., and G.J.P.L. Kops. 2018. Leader of the SAC: molecular mechanisms of Mps1/TTK regulation in mitosis. *Open Biol.* 8:180109. <https://doi.org/10.1098/rsob.180109>
- Qian, J., C. Winkler, and M. Bollen. 2013. 4D-networking by mitotic phosphatases. *Curr. Opin. Cell Biol.* 25:697–703. <https://doi.org/10.1016/j.cob.2013.06.005>
- Qian, J., M.A. Garcia-Gimeno, M. Beullens, M.G. Manzione, G. Van der Hoeven, J.C. Igual, M. Heredia, P. Sanz, L. Gelens, and M. Bollen. 2017. An Attachment-Independent Biochemical Timer of the Spindle Assembly Checkpoint. *Mol. Cell.* 68:715–730.e5. <https://doi.org/10.1016/j.molcel.2017.10.011>
- Santaguida, S., A. Tighe, A.M. D'Alise, S.S. Taylor, and A. Musacchio. 2010. Dissecting the role of MPS1 in chromosome biorientation and the spindle checkpoint through the small molecule inhibitor reversine. *J. Cell Biol.* 190:73–87. <https://doi.org/10.1083/jcb.201001036>
- Saurin, A.T., M.S. van der Waal, R.H. Medema, S.M. Lens, and G.J. Kops. 2011. Aurora B potentiates Mps1 activation to ensure rapid checkpoint establishment at the onset of mitosis. *Nat. Commun.* 2:316. <https://doi.org/10.1038/ncomms1319>
- Schindelin, J., I. Arganda-Carreras, E. Frise, V. Kaynig, M. Longair, T. Pietzsch, S. Preibisch, C. Rueden, S. Saalfeld, B. Schmid, et al. 2012. Fiji: an open-source platform for biological-image analysis. *Nat. Methods.* 9: 676–682. <https://doi.org/10.1038/nmeth.2019>
- Schmidt, J.C., T. Kiyomitsu, T. Hori, C.B. Backer, T. Fukagawa, and I.M. Cheeseman. 2010. Aurora B kinase controls the targeting of the Astrin-SKAP complex to bioriented kinetochores. *J. Cell Biol.* 191:269–280. <https://doi.org/10.1083/jcb.201006129>
- Stucke, V.M., H.H. Silljé, L. Arnaud, and E.A. Nigg. 2002. Human Mps1 kinase is required for the spindle assembly checkpoint but not for centrosome duplication. *EMBO J.* 21:1723–1732. <https://doi.org/10.1093/emboj/21.7.1723>
- Suijkerbuijk, S.J., M. Vleugel, A. Teixeira, and G.J. Kops. 2012. Integration of kinase and phosphatase activities by BUBR1 ensures formation of stable kinetochore-microtubule attachments. *Dev. Cell.* 23:745–755. <https://doi.org/10.1016/j.devcel.2012.09.005>
- Tighe, A., V.L. Johnson, and S.S. Taylor. 2004. Truncating APC mutations have dominant effects on proliferation, spindle checkpoint control, survival and chromosome stability. *J. Cell Sci.* 117:6339–6353. <https://doi.org/10.1242/jcs.01556>
- Tyler, R.K., M.L. Chu, H. Johnson, E.A. McKenzie, S.J. Gaskell, and P.A. Eyers. 2009. Phosphoregulation of human Mps1 kinase. *Biochem. J.* 417:173–184. <https://doi.org/10.1042/BJ20081310>
- Vallardi, G., L.A. Allan, L. Crozier, and A.T. Saurin. 2019. Division of labour between PP2A-B56 isoforms at the centromere and kinetochore. *eLife.* 8:e42619. <https://doi.org/10.7554/eLife.42619>
- Wang, X., H. Yu, L. Xu, T. Zhu, F. Zheng, C. Fu, Z. Wang, and Z. Dou. 2014. Dynamic autophosphorylation of mps1 kinase is required for faithful mitotic progression. *PLoS One.* 9:e104723. <https://doi.org/10.1371/journal.pone.0104723>
- Xu, P., E.A. Raetz, M. Kitagawa, D.M. Virshup, and S.H. Lee. 2013. BUBR1 recruits PP2A via the B56 family of targeting subunits to promote chromosome congression. *Biol. Open.* 2:479–486. <https://doi.org/10.1242/bio.20134051>
- Zeng, K., R.N. Bastos, F.A. Barr, and U. Gruneberg. 2010. Protein phosphatase 6 regulates mitotic spindle formation by controlling the T-loop phosphorylation state of Aurora A bound to its activator TPX2. *J. Cell Biol.* 191:1315–1332. <https://doi.org/10.1083/jcb.201008106>
- Zhu, T., Z. Dou, B. Qin, C. Jin, X. Wang, L. Xu, Z. Wang, L. Zhu, F. Liu, X. Gao, et al. 2013. Phosphorylation of microtubule-binding protein Hec1 by mitotic kinase Aurora B specifies spindle checkpoint kinase Mps1 signaling at the kinetochore. *J. Biol. Chem.* 288:36149–36159. <https://doi.org/10.1074/jbc.M113.507970>